Peer-reviewed version available at *Polymers* **2019**, *11*, 760; doi:10.3390/polym11050760

Design and Fabrication of Strong Parts from Biodegradable Polymer with a Desktop 3D Printer

Vladimir E. Kuznetsov[1], Azamat Tavitov, Oleg Urzhumtsev, Mikhail Mikhailin and Alexey N. Solonin

Department of Physical Metallurgy of Non-Ferrous Metals, National University of Science and Technology "MISIS", Leninskiy Prospekt 4, NUST MISIS, Moscow 119049, Russia

Abstract

The parts obtained by FFF technology are anisotropic in any direction; while the whole part constitutes out of layers, each of the layers include one or more perimeters of shell and the infill with density from 0 to 100%. Mechanical performance of FFF parts depends on its shape, orientation, constitution and 3D printing parameters.

A classification for shapes of parts obtained by FFF and stressed during its operation is provided. For the most questionable class (parts with interrupted shell critically stressed on interlayer boundaries) a representative sample and testing apparatus is developed. Different approaches to the sample shape modification were applied and tested. The part shape optimization resulted in increment of the force, required to fracture the part from 483 to 1096 N.

Keywords: design for additive manufacturing; desktop 3D printing; fused filament fabrication; polylactic acid; mechanical strength

In the current work, the following notions are introduced and the following shorthands are used:

FDM — Fused Deposition Method is a technology of digital additive manufacturing based on layered deposition of melted thermoplastic;

FFF – Fused Filament Fabrication, same as FDM with the only difference is that the *FDM* is a trademark of Stratasys Inc., while the *FFF* is a term coined inside the RepRap community. Since the current study involves open-source 3D printer, the term FFF is used;

Filament — plastic in the filament form used as supply in *FFF* process;

Thread — extruded and deposited thread of plastic mimicking the FFF part;

Shell — a component of FFF part, reproducing the lateral surface of 3D model. The shell of a layer consist of single or multiple equidistant perimeters formed by the thread. Number of perimeters and the thread widness are responsible for the shell thickness;

Infill — an internal component of FFF part, formed by threads in orthogonal straight lines. The distance between the threads describes the infill density;

Base — a component of FFF part, reproducing flat surfaces parallel to the 3D printer bed. Base may consist of multiple layers, usually printed mutually orthogonally in XY directions, and can be disabled;

Fracture load, the load observed during mechanical testing at which the sample exhibits the first crack, in the context of the study, the fracture load is the sample strength;

Relative Strength — a ratio sample's *fracture load* to its mass;

Flow rate (mm³/s) — the volume of plastic delivered through the nozzle per unit time;

Printing speed or *Feed rate* — the speed of nozzle traveling across XY plane while extruding the plastic.

[1] Corresponding author, Email address: kuznetsovve@misis.ru

Peer-reviewed version available at Polymers 2019, 11, 760; doi:10.3390/polym11050760

1 Introduction

Modern digital additive fabrication machines or 3D printers, are often subdivided into "desktop" (personal), "professional" and "industrial" ones. The main criterion determining that the particular model belongs to a one or another segment is the cost of the device. So, the desktop machines usually cost up to US$5 000 (while most of them in this segment are below US$2,000) [1]. The cost of most "professional" models is denoted with five digits, and the "industrial" machine rates are of six digits. The category of desktop additive machines features devices based on resin curing [2] and even on laser sintering [3], but the absolute majority of them are working on the principle of FDM [4,5,6], or FFF [7]. The broad spread of FFF technology has happened in the last decade thanks to the RepRap [8,9,10] and other open projects.

Due to the low cost of devices and consumables for them, the desktop FFF 3D printers can sometimes compete with traditional production processes. A single desktop 3D printer remains an extremely slow production tool, but its unlimited technological flexibility allows efficient scaling of performance by simply increasing the number of devices. A small business with 10 to 30 3D printers can effectively compete in the market for fast production of small batches with companies using the technology of vacuum molding of plastics or RIM. Thousands of 3D printers owned by individual users can quickly accept the order to manufacture a batch of thousands of parts using platforms such as 3d hubs [11]. The potential of desktop (home, amateur or personal) devices is huge. There are around 380 million tons of plastics of all kinds produced in the world annually [12], which means that about 50 kg of products made of plastic are consumed per one inhabitant of the planet. An average desktop device based on FFF technology is able to squeeze up to 5 mm^3 of polymer every second through a nozzle. Although not capable to operate continuously in the 24/7 mode, each of the printers is nevertheless potentially capable of annual production with a total mass of at least 100 kg. That means that productivity of a *personal* 3D printer can fulfill all the needs in plastic products of a *person*. While the Star Trek replicator is not yet invented, desktop machines seem to be suitable for the role of functional prototypes of future distributed manufacturing cells [13,14,15,16,17,18]. These machines have found its application in different fields, from science [24,25,26,27,28] to toys [29], from space [30,31] to farms [33]. However, until now it is hard to say that desktop 3D printers are widely considered as production tools. The limited use of desktop printers for manufacturing of functional parts capable to handle significant loads is largely caused by lack of trust for the new fabrication means by designers and engineers. This lack of trust is backed by the widespread belief that the strength of 3D printed parts is dramatically lower in comparison with parts manufactured using a traditional technology. Understanding the peculiarities of 3D printing technology and designing parts with keeping these peculiarities in mind, allows at least approaching the strength of monolithic polymer parts. There is significant amount of attention drawn to develop design rules for additive manufacturing [34,35] in order to achieve desired geometry. There are also some studies on the influence of parts topology on mechanical properties of FFF printed parts [36,37]. However, there is shortage in studies connecting 3D printed parts properties to their shape and constitution.

2 Problem statement

With all the variety of parts, the operation of which implies bearing mechanical loads and the manufacturing method is FFF 3D printing, they can all be divided into two categories (Figure 1) depending on stress state w.r.t. layer boundaries. It is assumed here and below that coordinate axes of the part are equal to the axes of the printer. The threads forming the part lie in the planes parallel to XY axes and thus orthogonal to the Z axis. The purpose, shape and printing orientation for the parts of the first category are such that the bonding strength between the layers does not play the critical role. In the part of the second category the weak spot, on the contrary, is situated on the layer boundary and the cohesion between the layers determines the strength of the whole part.

Peer-reviewed version available at Polymers 2019, 11, 760; doi:10.3390/polym11050760

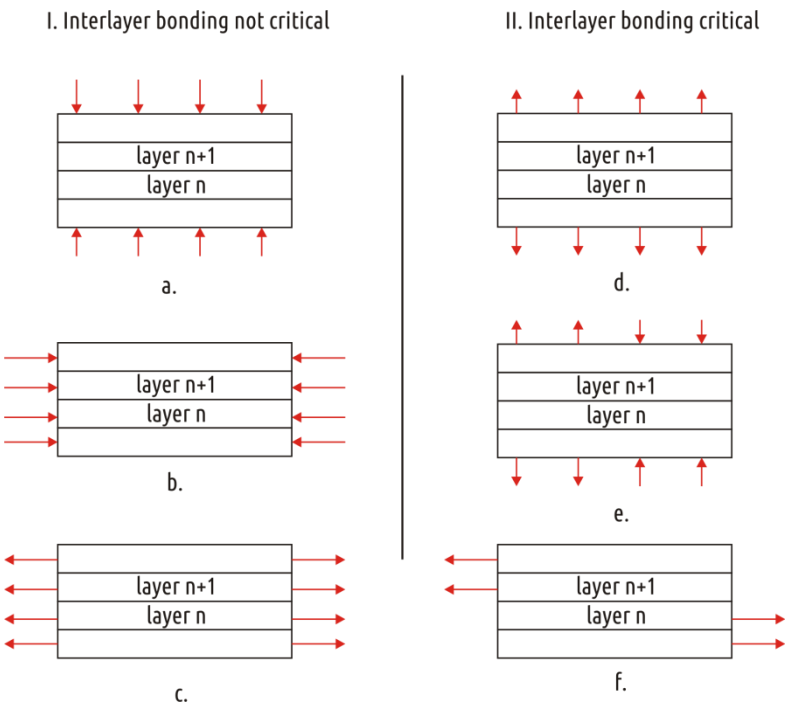

Figure 1. Two categories of stressed layered parts there interlayer bonding is not (I.) and is (II.) critical. The category I. includes cases of compression along the Z axis with no buckling (a) and compression (b) and tension (c) orthogonal to Z axis. The category II. includes cases of tension (d) and bending (e) along Z axis and torque or shear orthogonal to the Z axis (f)

The first category includes parts that are compressed along Z axis during operation and that do not experience risk of buckling (Figure 1, a), for example, the "amplifier flat stand" (https://www.thingiverse.com/thing:3475564). The first category also includes parts printed in such a way that critical stresses are applied along the layers (in the XY plane) and the stress state is almost independent from the Z axis coordinate (Figure 1, *b* and *c*), for example, "Knuckle Duster" (https://www.thingiverse.com/thing:596768) or "Bag Holder" (https://www.thingiverse.com/thing:26767). There are no questions on how to align such flat parts on the printer bed: the most stable position is the most appropriate regarding the stress distribution. Another type of models are, for example, "Fixing Angle" (https://www.thingiverse.com/thing:581036). They fall into this category only if correctly oriented w.r.t the printer bed with both corner shelves oriented parallel to the Z axis.

Like any products fabricated on a 3D printer, the parts from the first category will be layered and therefore anisotropic, but this anisotropy does not show up during their operation. Such parts' behavior under load will differ little from that one of parts of the same shape and material obtained by traditional methods, such as injection molding. Accordingly, shape optimization for such parts should use the accumulated experience in designing parts for traditional production methods. In this case 3D printing technology imposes certain restrictions (for example, the minimum element size, taking into account the nozzle diameter and printer accuracy), but at the same time it removes many of the limitations that are inherent for traditional production methods (there is no need for technological drafts and fillets, it is possible to create enclosed cavities etc.).

The second category comprises parts that stretch or bend along or twist around the Z-axis during operation (Figure 1 d, e, f). Such parts experience normal tensile stresses or tangential shear stresses acting on the layers boundaries.

With structural features of FFF printed parts taken into account, it makes sense to subdivide the second category into two.

The first subcategory includes parts with shell not being interrupted during the printing process: polymer threads forming the shell of the next layer lie completely or partially on the threads forming the shell of a previous layer. An example of such part is the "hammer"

Peer-reviewed version available at Polymers 2019, 11, 760; doi:10.3390/polym11050760

(https://www.youmagine.com/designs/3d-printed-hammer) or the “box spanner adapter” (https://www.youmagine.com/designs/box-spanner-adapter).
Such models cannot have more than two flat edges parallel to the XY plane, and these faces can be located only at the very bottom and at the very top of the part. The strength this subcategory of parts is determined primarily by the strength of its shell. Accordingly, a simple and efficient recipe for increasing the strength of such parts is to invest material and printing time into shell formation. Infill should be considered as support for the upper horizontal base in this case. In case such support is not necessary, there is no point in wasting time and material printing the infill — it is better to use these resources to add one or more extra perimeters of the shell. Ways to increase the shell strength (layer cohesion) for PLA FFF parts are studied in [38,39].
Finally, the second subcategory comprises parts which have a shell that is interrupted one or more times during the printing process, that is, there are times when the threads forming the shell of the next layer lie on the filaments forming the base, infill or support. Such models can be exemplified by the “Spool holder” (https://www.thingiverse.com/thing:408288), Plane Handle (https://www.thingiverse.com/thing:2172679) or the “Hook” (https://www.thingiverse.com/thingUE004805). These parts have flat faces parallel to the XY plane outside the upper and lower bases of the part. Examples of parts of all the categories and subcategories considered are shown on Figure 2.

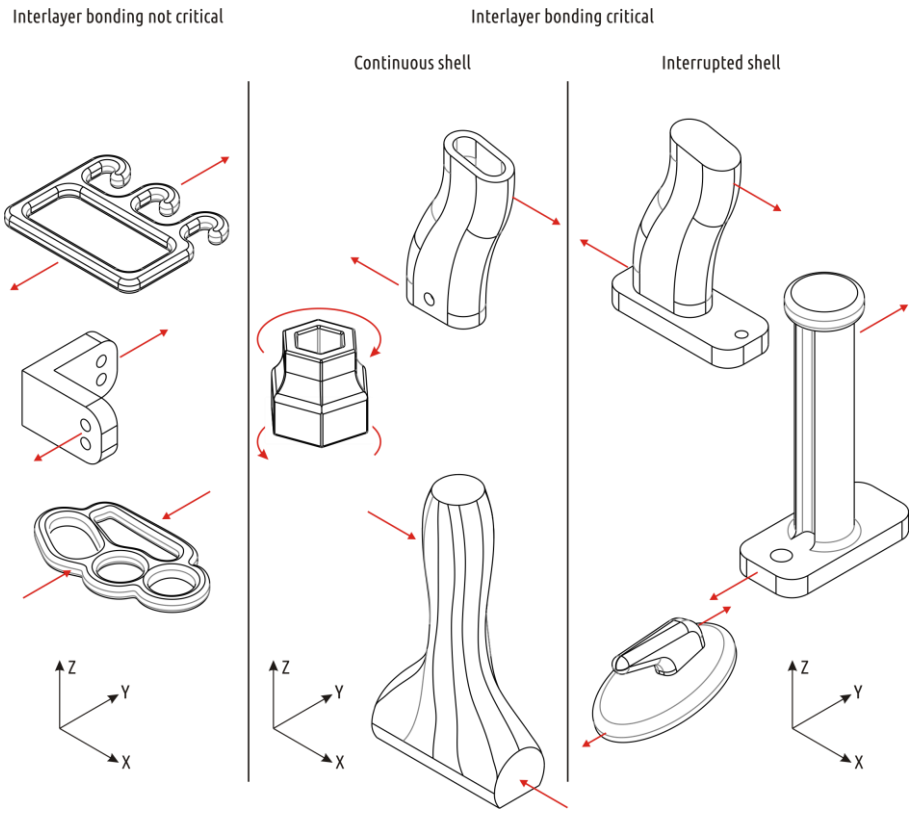

Figure 2. Examples of 3D printed parts experiencing significant stress during operations

Behavior of critically stressed parts with shell interruptions (II b.) seems to be the least predictable in comparison with overs (I and II a.). The hypothesis is that the interruption of shell in the most stressed area of a loaded 3D printed part will result in parts’ unacceptably low mechanical performance. Thus, the current work is devoted to the study of parts with interrupted shells and the ways to increase the strength of such parts by modifying its shape with respect to its constitution.
The study is made on samples 3D printed of poly (lactic acid), or PLA, which currently is one of the most popular materials for FFF. The main advantage of PLA in comparison to other polymers and blends used for FFF 3D printing is the low level of shrinkage and relatively low melting temperature. Another advantages of PLA include its biodegradability, absence of

Peer-reviewed version available at Polymers 2019, 11, 760; doi:10.3390/polym11050760

unpleasant odors when heated, and its overall environmental compatibility in all aspects of the life cycle. PLA emits ten times less potentially dangerous ultra-fine particles [40] than ABS and can withstand at least 25 kiloGray of gamma irradiation with no degradation of mechanical properties [41]. Perhaps, the only important disadvantage of the PLA is its relatively low Vicat point, which makes it incompatible with elevated temperature environment.

3 Methods and materials

3.1 Sample shapes

An item consisting of two connected coaxial cylinders of large (boss) and small (shaft) diameters was selected as a representative of part with an interrupted shell (Figure 3a). As a test procedure radial load is applied to the shaft with the boss is rigidly fixed (Figure 3b). Obviously, the most loaded (and weakest) area of the part is the junction between the shaft and the boss (the place there shell is interrupted).

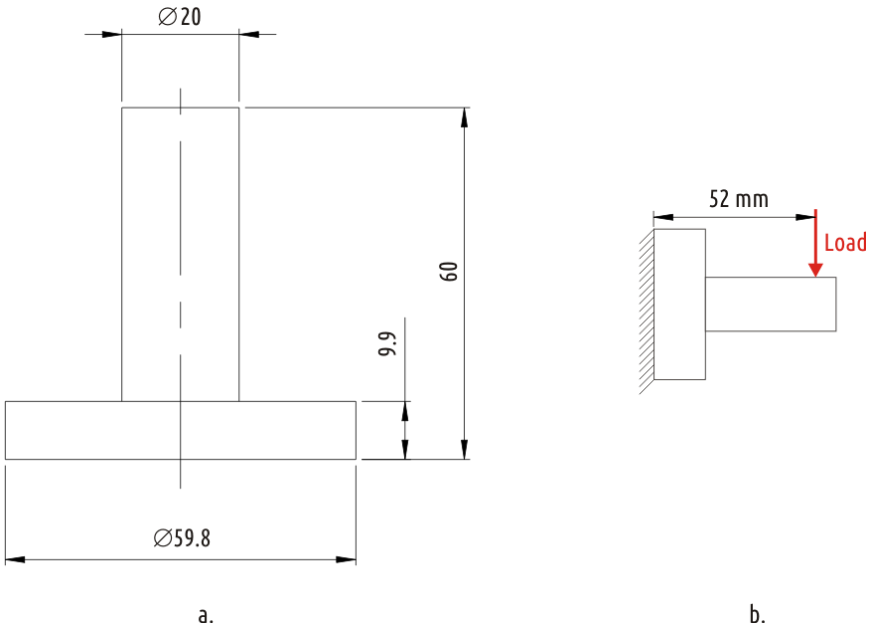

Figure 3. Basic sample dimensions (a) and loading (b) scenario

Based on the shape described above and keeping main dimensions intact, four extra CAD models were prepared and tested in attempts to improve the part mechanical performance (Figure 4).

Peer-reviewed version available at Polymers 2019, 11, 760; doi:10.3390/polym11050760

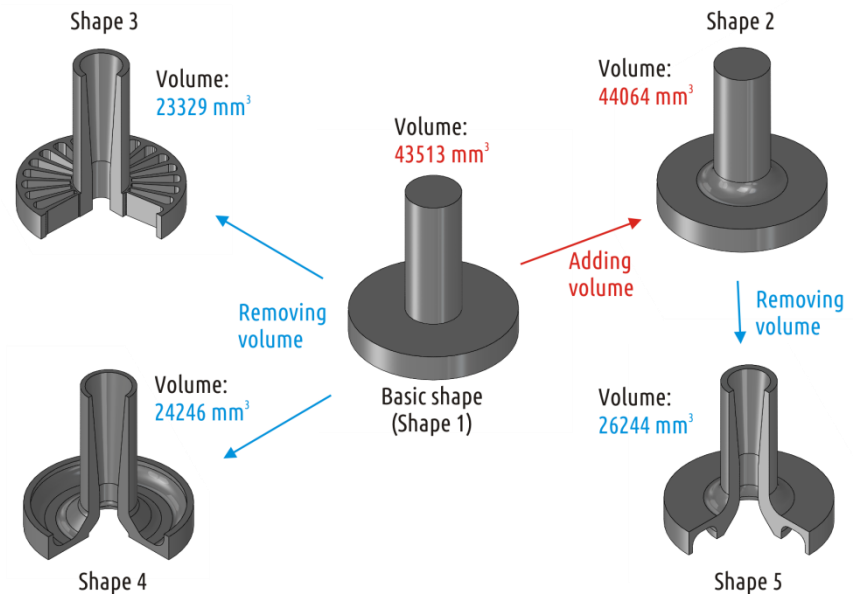

Figure 4. Part shapes studied

For CAD models with relatively large volume (Shape 1 and Shape 2) eight different configurations were tested. Three parameters describing 3D printed part constitution were varied at two levels: shell thickness (1.2 and 2.4 mm), base thickness (0.6 and 1.2 mm), and infill value (20 and 60%). For CAD models with lower volume a single configuration was tested: shell thickness 1.8 mm, 100% infill and no bases (base thickness 0 mm).

3.2 Samples fabrication

A desktop Ultimaker 2 (Ultimaker B.V., Geldermalsen, The Netherlands) printer was used to produce all the samples. The specific machine used differs from the mass-market model with an installed alternative feed mechanism of BondTech (Bondtech AB, Värnamo, Sweden) brand, built on a stepper motor with an integrated gearbox and drive to both feed rollers, and an alternative 3D Solex (Cepta AS, Norway) heating unit with an increased power heating element (~ 50 W). The alternative heating unit, unlike the stock one, allows changing nozzles. In this series of experiments, a brass nozzle with a channel diameter of 0.6 mm was used instead of the 0.4 mm standard nozzle in stock Ultimaker 2 hot end.
A turquoise PLA filament of 2.85 mm in diameter was used, produced by REC Company (Moscow, Russia). All the material came from the same batch produced in June 2018, according to the labels (6 months before the experiment). The filament was supplied on standard spools of 750 g net weight, samples printing used about 550 - 650 g of each spool (the inner turns of the coils are usually harder to unwind, which can lead to a decrease in extrusion efficiency and adversely affect the weight and strength of the samples).
This specific manufacturer of filament was chosen due to locally produced material and the desire to obtain results comparable with previous studies [38,39]. Papers [42,38] show that all other characteristics being identical the filament color influences strength characteristics of the products made from it. Thus, filament of the same color was used as in previous studies.

The values of the printing parameters remained constant during all experiments:

- extrusion temperature (210 °C);
- nozzle diameter (0.6 mm);
- heated bed temperature (60 °C);
- first and subsequent layer thickness (0.3 mm);
- first layer printing speed (25 mm/s);
- subsequent layers printing speed (30 mm/s);
- flow rate (5.4 mm^3/s).

Peer-reviewed version available at Polymers 2019, 11, 760; doi:10.3390/polym11050760

For each observation mentioned in the work, a lot of five samples was made and tested. The paper presents the average values for each test lot, while the standard deviation is indicated after the average value in brackets.
The sample was placed at the center of the printer bed. The G-code file was prepared using Cura 15.02.1 software (slicer).

3.3 Sample mass measurement

All samples were weighed before mechanical testing using digital analytical scales ViBRA LF Series (Shinko Denshi Co. LTD, Japan). Measurement results were rounded to one decimal digit.

3.4 Mechanical Testing

Sample strength tests were carried out on a standard universal electromechanical testing machine IR 5057-50 (OOO Tochpribor, Ivanovo, Russia) with a digital control system. The samples were fixed with a specially designed and manufactured device (Figure 5). That fixture was mounted on a movable traverse of the testing machine. The top roller from the three-point bend test kit was used to apply load on the sample shaft.

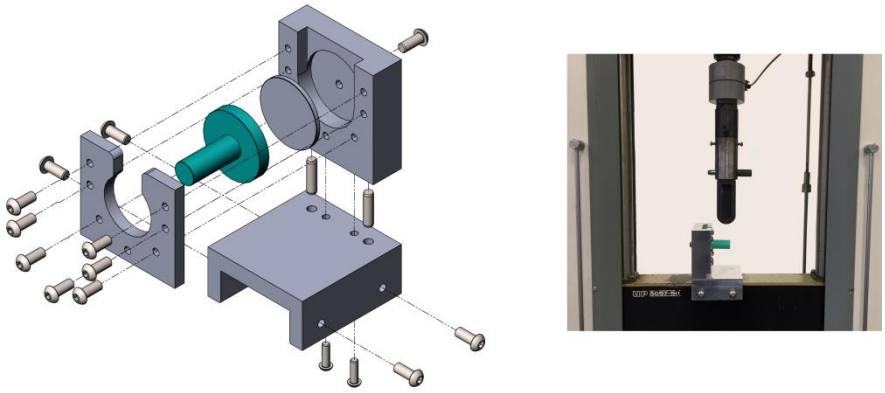

a. b.

Figure 5. Sample fixture (a) installed on the universal testing machine (b)

The tests were carried out at constant speed (10 mm/min), and were held on until the sample was destroyed. During the tests displacements and loads were recorded. The reference point was the state of the machine with a load of 5N applied to eliminate mounting clearances.
The part strength was assumed to be equal to the fracture load (load at which the first apparent crack appears). That point can be easily displayed on the load-displacement curve. Along with absolute strength, the relative strength (fracture load related to the sample mass) was also considered.

4 Results and discussion

4.1 Basic shape

The solid geometry of any model is interpreted by the slicer as a combination of a shell, upper and lower horizontal bases and infill inside it. The shape considered contains all three geometric components in the critical zone, at the junction of the shaft and boss (Figure 6).

Peer-reviewed version available at Polymers 2019, 11, 760; doi:10.3390/polym11050760

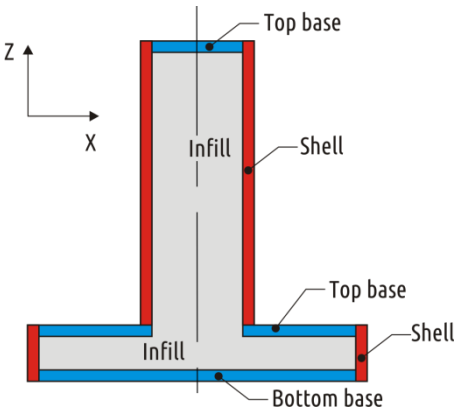

Figure 6. Shape 1 and its constitution

To assess how do these three geometric components contribute to the part strength, they were varied at two levels. The test results for eight configurations of Shape 1 are shown in the Table 1.

Table 1. Test results for Shape 1 configurations

#	Code	Shell, mm	Base, mm	Infill, %	Sample mass, g *	Fracture load, N	Relative strength, N/g
1	S12B06F20**	1.2	0.6	20	17.6 (0.1)	187 (13)	10.6
2	S12B06F60	1.2	0.6	60	33.4 (0.2)	365 (24)	10.9
3	S12B12F20	1.2	1.2	20	21.0 (0.1)	275 (18)	13.1
4	S12B12F60	1.2	1.2	60	34.9 (0.2)	462 (24)	13.2
5	S24B06F20	2.4	0.6	20	22.1 (0.1)	201 (28)	9.1
6	S24B06F60	2.4	0.6	60	35.6 (0.1)	357 (23)	10.0
7	S24B12F20	2.4	1.2	20	24.8 (0.1)	290 (28)	11.7
8	S24B12F60	2.4	1.2	60	36.9 (0.2)	483 (27)	13.1

* - hereinafter, the values in brackets are standard deviations

** - hereinafter S — shell, B — base, F — infill

The loading curves of the characteristic representatives for each of the lots tested are shown in the Figure 7.

Peer-reviewed version available at Polymers 2019, 11, 760; doi:10.3390/polym11050760

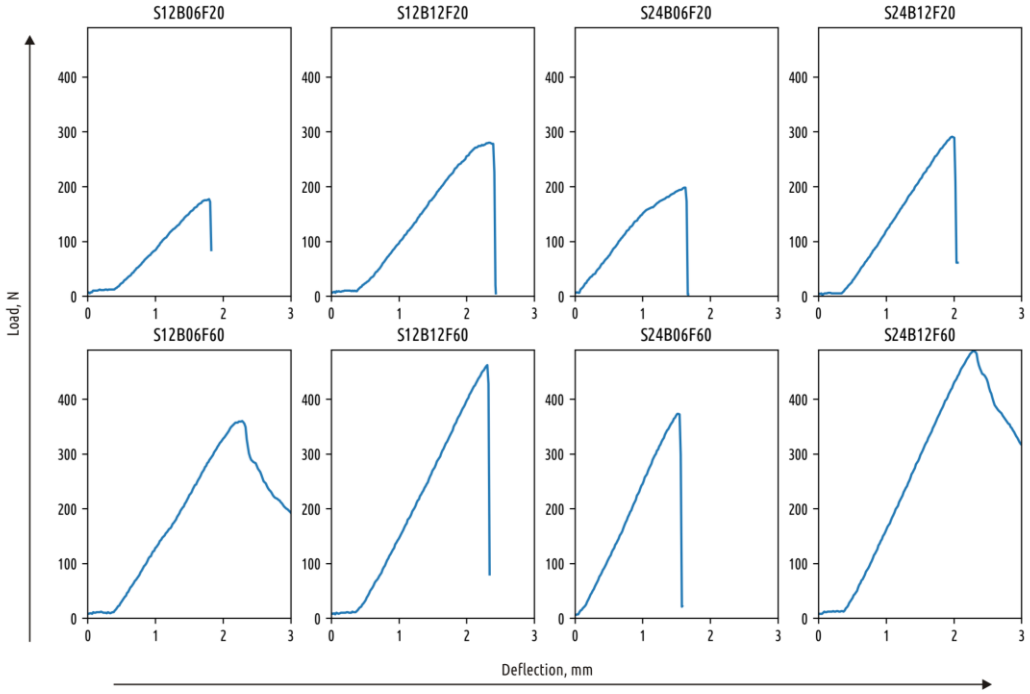

Figure 7. Examples of strength test curves for Shape 1 specimen manufactured in different configurations

In general, the strength of all the considered configurations is very modest. The shaft itself is quite durable, but it gets easily separated from the boss (all the samples examined were destroyed at the interface between the shaft and the boss, see Figure 8). The reason for this lies in the fact that the strong shaft stands on the loose base of the thread grid forming the boss infill. The connection between the shaft and the boss passes through the infill and along the boundary between the upper base of the boss and the shaft shell. In simple words, the part is weak due to the shell interruption.

Peer-reviewed version available at Polymers 2019, 11, 760; doi:10.3390/polym11050760

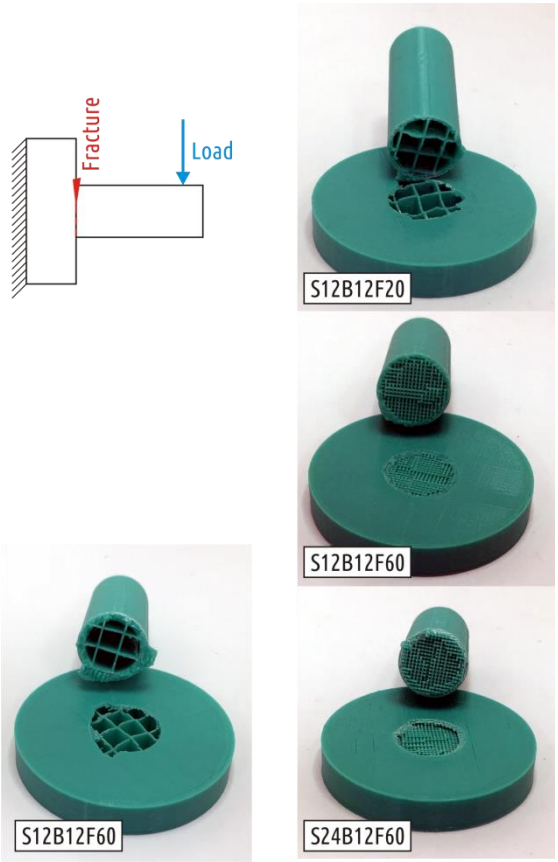

Figure 8. Fracture of Shape 1 samples

As it can be seen from the Figure 9, increasing the base thickness and infill percentage has noticeable effect on the part strength, while the shell thickness has the minimal influence. Thus, the rule that works well for parts with a continuous shell (in order to increase the part strength it is necessary first of all to invest time and material into shell) is absolutely inapplicable to parts of the shape considered.

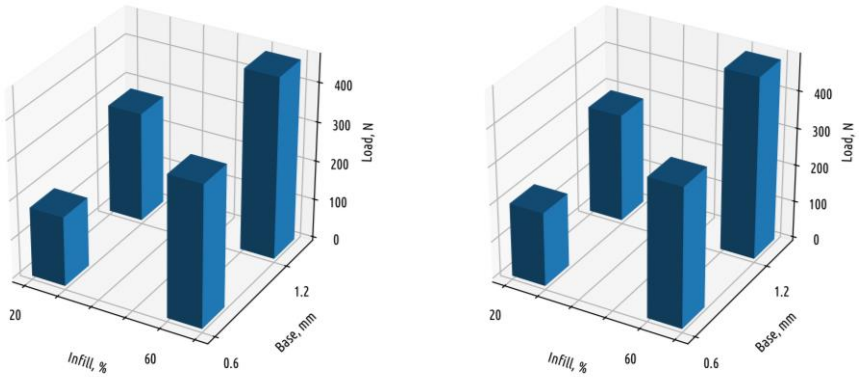

a. *b.*

Figure 9. Fracture load depending on base thickness and infill density for samples of Shape 1 with shell thickness equal to 1.2 (a) and 2.4 (b) mm

Acceptable values of part strength can be achieved by further increasing the infill value (up to 100%), but this will obviously lead to significant increase in the part mass. Considering relative values and comparing samples that only differ by infill parameters one can see that increasing infill density from 20% to 60% leads to a negligible increase in relative strength due to significant increase in total sample weight.

Peer-reviewed version available at Polymers 2019, 11, 760; doi:10.3390/polym11050760

A more rational way is to modify the part shape while keeping the main (coupling) dimensions intact.

4.2 Shape modification — the traditional approach (Shape 2)

The most obvious solution for increasing the part strength by modifying the shape is to add a fillet to the base of the shaft. The fillet literally rounds the sharp transition, removing the apparent stress concentrator at the junction between the flat boss and the cylindrical surface of the shaft, and also adds material to the most loaded area of the part. Adding a fillet with a radius of 6 mm leads to an increase in total part volume of 550 cubic mm and significantly increases the interface area between the shaft and boss (Figure 10).

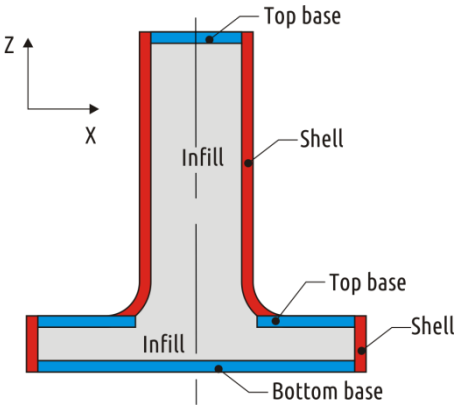

Figure 10. Shape 2 and its constitution

The test results for eight configurations of Shape 2 are shown in the Table 2, and characteristic loading curves are presented in the Figure 11.

Table 2. Test results for Shape 2 configurations

#	Code	Shell, mm	Base, mm	Infill, %	Mass, g	Fracture load, N	Relative strength, N/g
1	S12B06F20	1.2	0.6	20	20.0 (0.1)	508 (30)	25.4
2	S12B06F60	1.2	0.6	60	34.1 (0.2)	648 (12)	19.0
3	S12B12F20	1.2	1.2	20	21.3 (0.2)	506 (36)	23.8
4	S12B12F60	1.2	1.2	60	35.4 (0.2)	650 (28)	18.4
5	S24B06F20	1.2	0.6	20	23.6 (0.1)	620 (36)	26.3
6	S24B06F60	2.4	0.6	60	35.9 (0.2)	896 (38)	25.0
7	S24B12F20	2.4	1.2	20	24.9 (0.2)	644 (45)	25.9
8	S24B12F60	2.4	1.2	60	37.2 (0.2)	906 (52)	24.4

Peer-reviewed version available at Polymers 2019, 11, 760; doi:10.3390/polym11050760

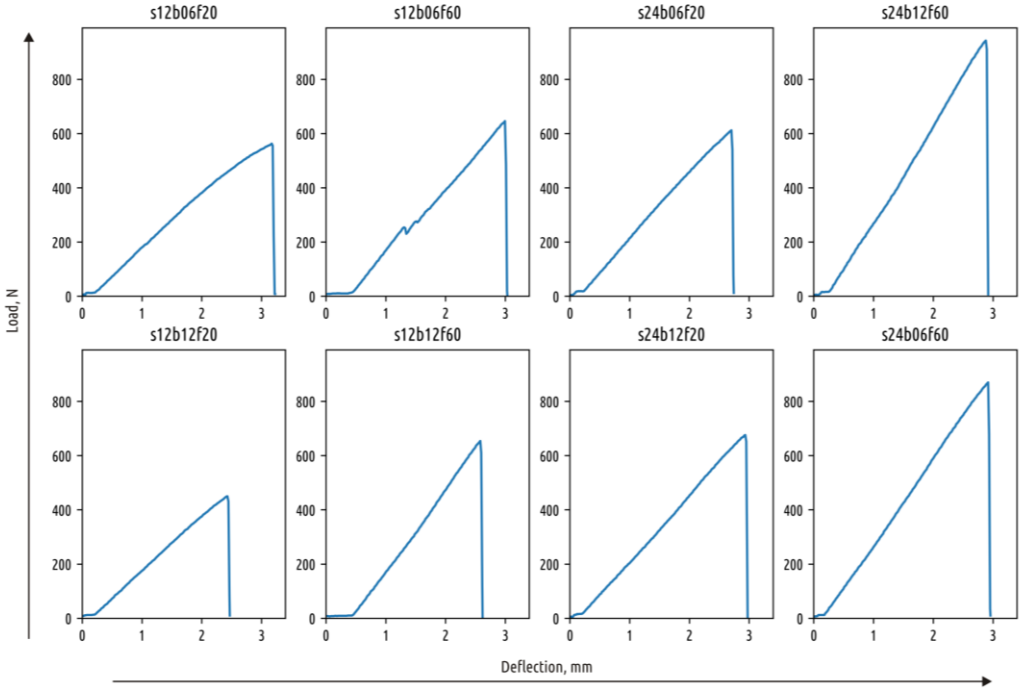

Figure 11. Examples of strength test curves for Shape 2 specimen manufactured in different configurations

As can be seen from the results, the simple addition of a fillet dramatically affects the strength of the part. The smallest recorded strength for Shape 2 samples exceeds the maximum recorded one for Shape 1. Moreover, the nature of parameter influence changes completely. Samples with thicker shells (2.4 mm) and low infill density (20%) break at the interface between the boss and fillet. All others fail at the boundary between the fillet and the cylindrical part of the shaft (Figure 12).

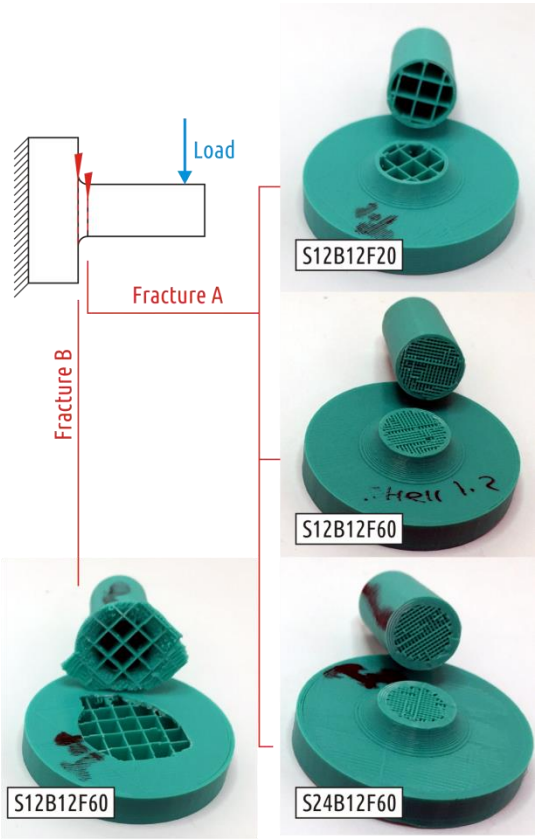

Peer-reviewed version available at Polymers 2019, 11, 760; doi:10.3390/polym11050760

Figure 12. Two types of Shape 2 samples fracture

Accordingly, in most cases the base thickness does not have any influence, since the material forming the base does not lie in the critical zone. The difference in results between samples that only vary in base thickness is statistically insignificant. Thus the number of configurations of Shape 2 samples can be reduced from 8 to 4 (Figure 13).

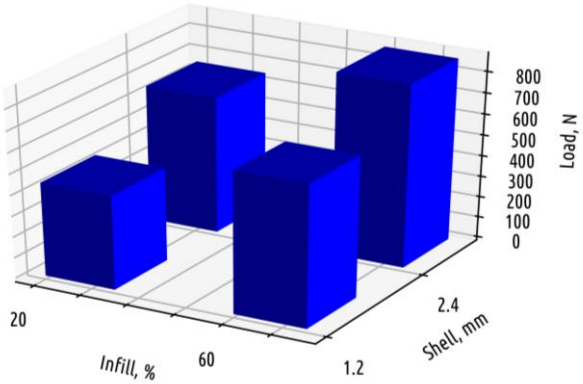

Figure 13. Fracture load depending on base thickness and infill density for samples of Shape 2

The infill density has a great influence on the absolute part strength for Shape 2, but for the relative strength shell thickness becomes paramount: increase in the infill rate from 20 to 60% with other things remaining unchanged leads to a decrease in the relative part strength. The best absolute result was achieved on the sample with the largest mass (infill density 60%, shell thickness 2.4 mm, base thickness 1.2 mm)

4.3 Modifying the shape with FFF technology specificity in mind (Shape 3)

When working with traditional manufacturing methods, whether it is molding, casting, forming or machining, it is impossible to make the part stronger by removing some of the CAD model volume. Removing the material from the least loaded areas can increase the relative (specific) strength of the part, that is, without or with a slight decrease in the strength it is possible to achieve significant reduction in weight, but it is impossible to increase the absolute strength by removing the material. In the case of the FFF technology removing some of the part volume from the CAD model does not necessarily imply reduction of the physical product mass. Slicer turns any CAD model into a combination of a shell, bases and infill, the appearance of additional open or closed cavities in the model leads to the appearance of additional shells in the slicer (and in the part printed). This feature of FFF can and should be used when designing strong parts.
The Figure 14 shows the modified model (Shape 3): external dimensions are preserved same to the base shape (Shape 1), but axial and radial cuttings are added.

Peer-reviewed version available at Polymers 2019, 11, 760; doi:10.3390/polym11050760

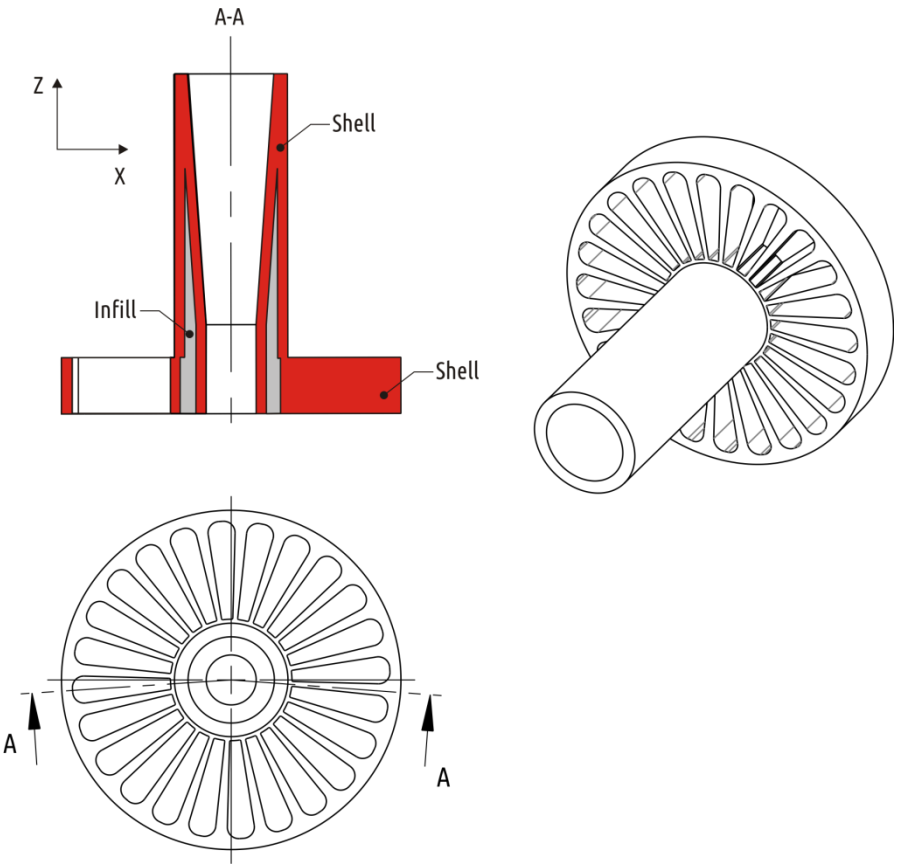

Figure 14. Shape 3 constitution

As a result of these changes, thread deposition paths are generated completely differently: the shaft shell is now passes through the boss and is printed from the very printer table; in fact, the shell becomes continuous. The cuts added to the model make it possible to fill the remaining parts of it as tightly as possible with plastic while maintaining the part mass within the limits achieved with the basic shape (Shape 1). The characteristic test curve is shown in the Figure 15. Sample destruction occurred over the shaft section, slightly submerged (1-3 mm) into the boss (Figure 16).

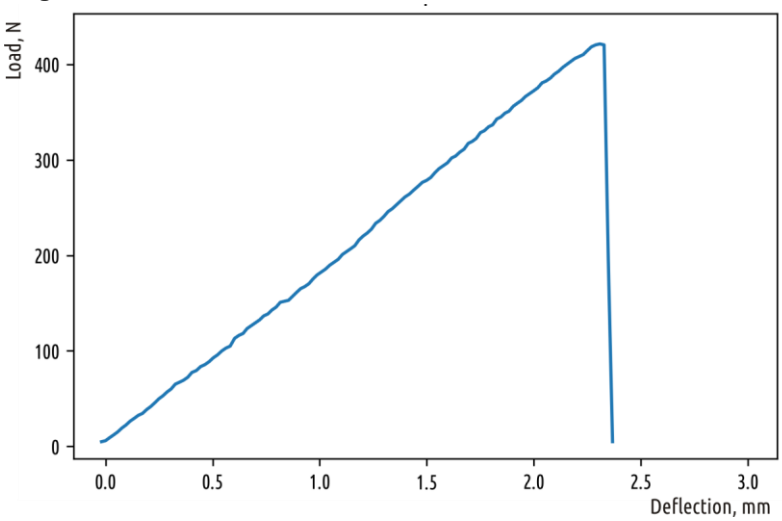

Figure 15. Typical loading curve of Shape 3 samples

Peer-reviewed version available at Polymers 2019, 11, 760; doi:10.3390/polym11050760

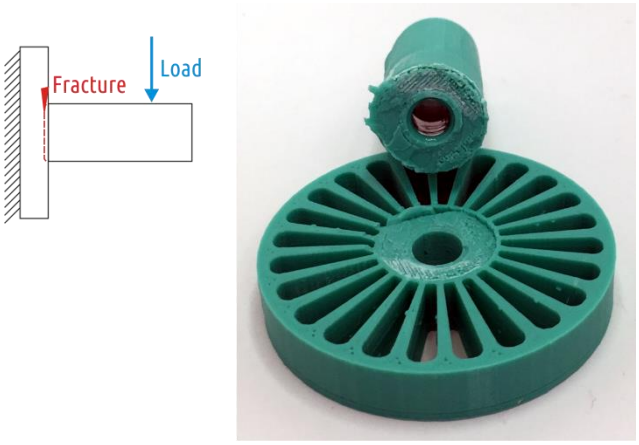

Figure 16. Fracture of Shape 3 samples

The average absolute strength of Shape 3 samples was 426 (18) N with a mass of 27.0 (0.1) g. The relative strength of the part was accordingly 15.8 N/g. The results obtained are inferior to the best absolute records obtained for Shape 1 but exceed the best relative ones. The results are significantly inferior to those obtained for Shape 2. It is important to note that Shape 3 fits into the basic shape volume, while Shape 2 has an element (fillet) protruding beyond its dimensions.

4.4 Shape optimization using CAE (Shape 4)

The Shape 1 and Shape 2 printed samples are far from solid bodies in their structure: they consist of dense bases, shell and loose infill. Using traditional methods of computer simulations to calculate the stress-strain state in such parts will not give an adequate result. On the other hand, the Shape 3 sample is formed exclusively from the shell and 100% infill. Such a part will not be completely solid — there will be discontinuities along the boundaries between individual plastic threads, but with some assumptions such an object can already be considered a solid body and can be analyzed with computer-aided simulation techniques. An example of adequate numeric simulation of loaded 3D printed PLA part can be found in [21]. In current paper, the SolidWorks Simulations extension of SolidWorks 2017 was used. The Figure 17 shows the stress distribution in the loaded areas of Shape 3. It can be seen that the boss is almost not loaded, and the critical stresses are concentrated at the junction of the boss and the shaft, where failure occurs.

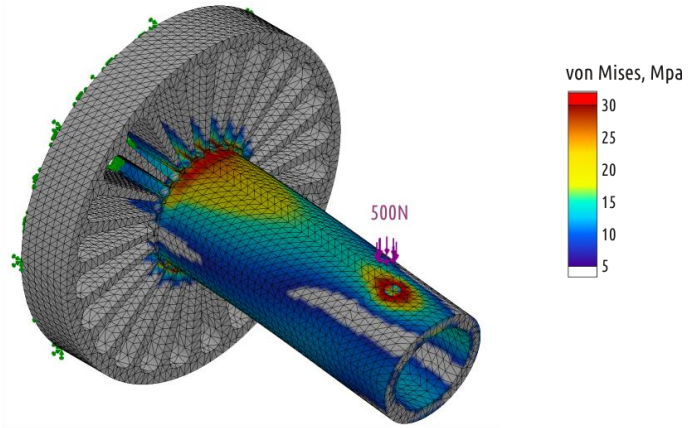

Figure 17. Stress distribution in the Shape 3 (SolidWorks Simulations)

After several cycles of shape modification and stress analysis, the Shape 4 was designed, where the calculated stresses are distributed between the shaft and the base (Figure 18). At the same time, it fully fits into the volume of the basic shape, like Shape 3 does (Figure 19).

Peer-reviewed version available at Polymers 2019, 11, 760; doi:10.3390/polym11050760

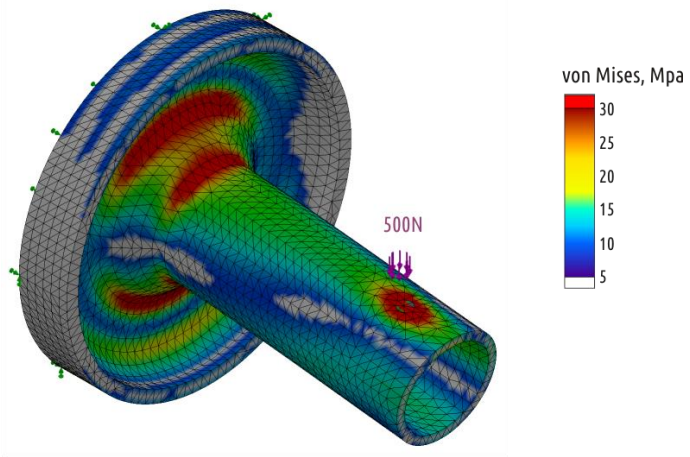

Figure 18. Stress distribution in the Shape 4 (SolidWorks Simulations)

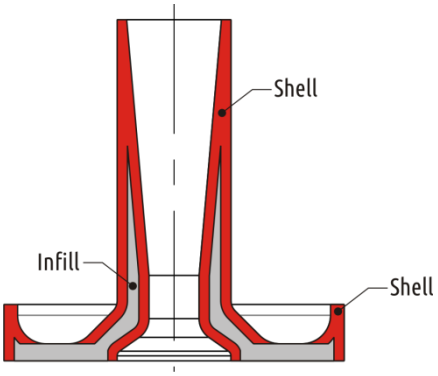

Figure 19. Shape 4 and its constitution

Due to the existence of a through hole along the shaft axis, there are two shells (like in Shape 3) instead of one in it (like it was in Shapes 1 and 2), the inner and the outer one. The inner shell of the Shape 4 part is continuous, and the outer shell is interrupted, but it stands on the 100% infill foundation.

In all previous cases, the load at which crack occurred was the largest load on testing curve. Four of the five tested Shape 4 samples showed another behavior under critical loads (Figure 20).

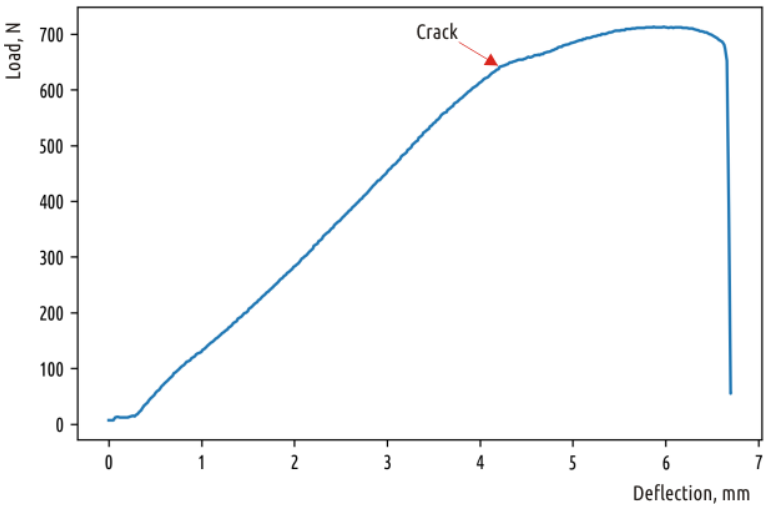

Figure 20. Typical loading curve for Shape 4

After the appearance of the first crack, the load required for further deformation continues to increase. That is, the appearance and growth of a crack does not immediately lead to the shaft separation from the boss, and the crack appears and grows in the boss part of the sample (Figure 20). One of the five tested specimens fractured at the point of transition of the

Peer-reviewed version available at Polymers 2019, 11, 760; doi:10.3390/polym11050760

cylindrical shaft into a conical inlet (Figure 21). If we come back to stress distribution in Figure 18, it can be seen that computer simulation revealed two critical zones. As the experiment showed, the sample destruction is possible in each of them with different probability.

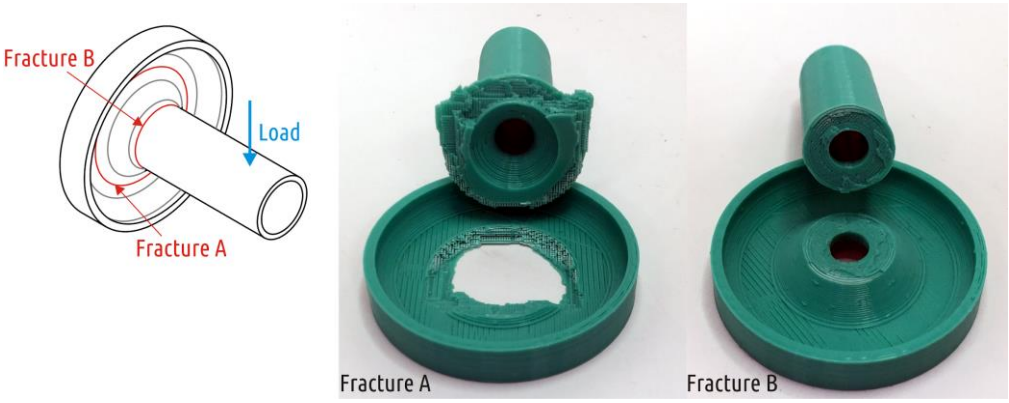

Figure 21. Two kinds of Shape 4 fracture

The more likely fracture (Figure 21, fracture A) passes through the entire boss that is formed by 100% infill. Due to the mutually orthogonal threads arrangement of different infill layers, the crack in the sample does not only grow along the borders between the individual plastic threads, but also across the threads. It is the latter phenomenon that ensures the ductile nature of sample destruction.

From the operational point of view, the destruction of a part of a machine or a mechanism by irrevocable deformation with rare exception is preferable to destruction by fragmentation. Further modification of the CAD model may redistribute stresses towards the boss from the shaft rather than contributes to their parity. The latter will somewhat reduce the part strength but will guarantee its gradual (ductile) destruction.

If the Shape 4 part strength is to be defined as the load corresponding to the crack appearance, the average strength is 662 (51) N with a mass of 27.6 (0.1) g.

In general, experiments with Shape 4 showed that when printing conditionally solid parts (not containing infill below 100%) their behavior becomes predictable by using computer simulations. Accordingly, not only intuitive assumptions can be used to modify and optimize the form, but also CAE tools. In addition, it is shown that changing the part shape can influence the nature of the destruction, in particular, from brittle to ductile.

4.5 Combining approaches (Shape 5)

Shape 1 can be considered an example of poor design: the sharp transition from the boss to the shaft is a flaw even for traditionally manufactured parts. In case of 3D printing, such a transition implies shell interruption and critical weak spot appearance. As it is shown by results for shapes 3 and 4, redistribution of material within a given, initially flawed, shape can significantly increase the part strength, but the geometry optimization effect taking into account 3D printing features is less significant than the effect of geometry modification performed in accordance with the basic principles of designing products for convenient manufacturing (samples of Shape 2).

The greatest effect can be achieved by combining a reasonable additions and subtractions of the volume in the CAD model being optimized. The Figure 22 shows Shape 5 obtained by removing the volume from the least loaded sections of the Shape 2.

Peer-reviewed version available at Polymers 2019, 11, 760; doi:10.3390/polym11050760

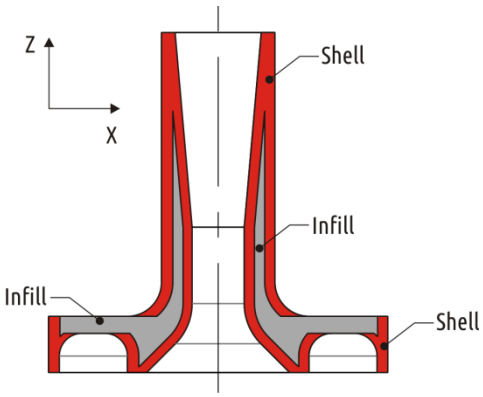

Figure 22. Shape 5 and its constitution

The fracture of all the tested samples occurred where the cylindrical shaft transitions into the fillet (Figure 23), the characteristic test curve is shown in the Figure 24.

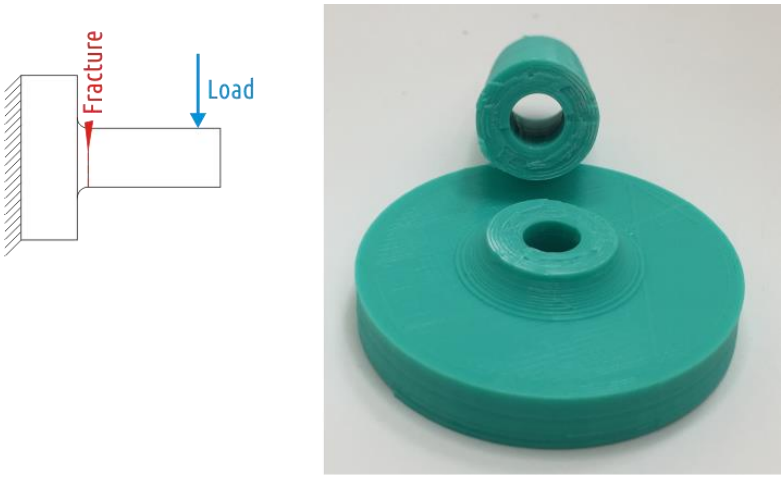

Figure 23. Shape 5 samples fracture

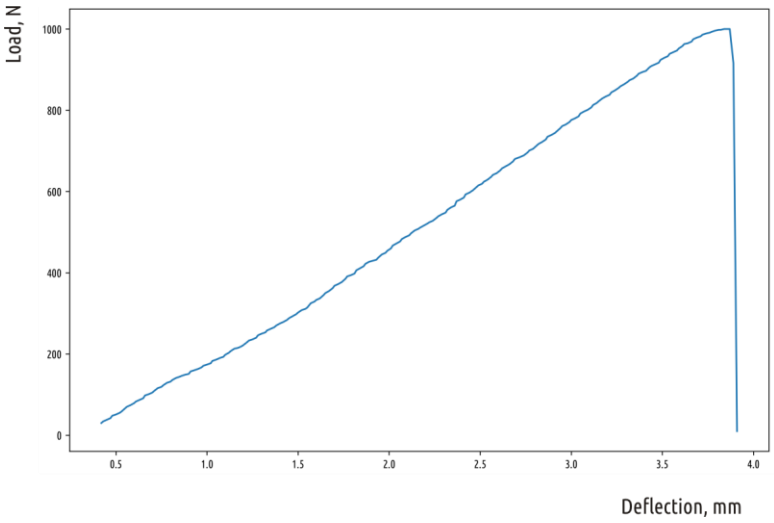

Figure 24. Typical loading curve for Shape 5

The average strength values for the Shape 5 samples amounted 1096 (72) N with a mass of 30.3 (0.2) g. The relative strength of the sample was 36.2 N/g.

Peer-reviewed version available at Polymers 2019, 11, 760; doi:10.3390/polym11050760

4.6 Summary

It is possible to significantly increase the part strength (Figure 25) by modifying its shape, based on an understanding of the FFF technology principles.

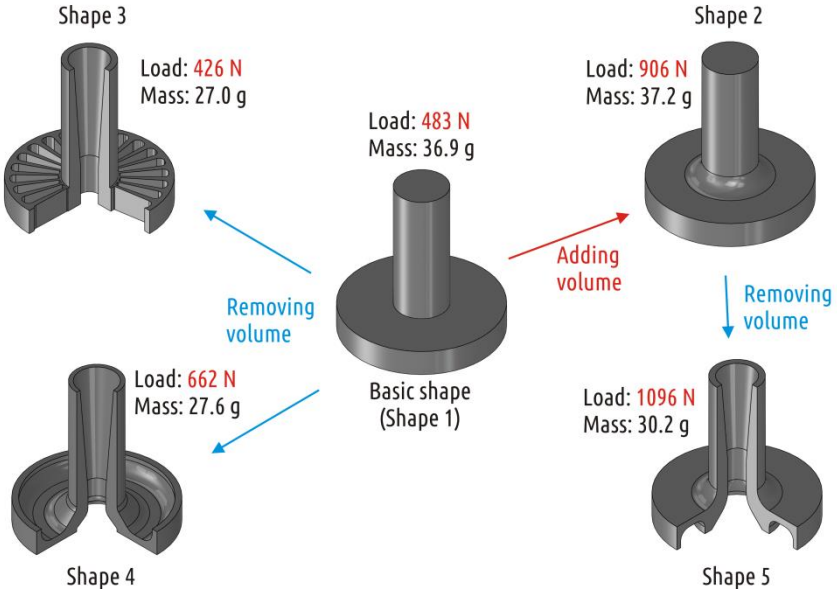

Figure 25. Shape optimization path and results

As a result of the shape modification without going beyond the initial geometric boundaries, it was possible to increase the strength (relative strength):

- for the model with a sharp transition between the boss and the shaft (Shape 1 to Shape 4) by 1.37 times (1.83 times);
- for the model with a smooth transition between the boss and the shaft (Shape 2 to Shape 5) by 1.13 times (1.40 times).

Additional reserves to improve the part strength for an optimized shape can be sought in technological parameters optimization of the printing process.

Conclusions

1. In order to increase FFF part strength its geometry can be optimized both by adding volume to the CAD model (rounding, adding fillets, smooth transitions), and by introducing cavities. This technique of shape optimization for the FFF production technology differs from that one for traditional production methods, as well as other digital additive technologies (SLA, SLS, LOM).
2. Computer simulation methods are applicable to analyze the behavior of FFF part models under load if they are printed with infill only with 100% density (or without infill invocation), at least at a qualitative level.

Acknowledgments

The work was carried out with financial support from the Ministry of Education and Science of the Russian Federation in the framework of increase Competitiveness Program of NUST “MISIS”, implemented by a governmental decree dated 16th of March 2013, No. 211

Peer-reviewed version available at Polymers 2019, 11, 760; doi:10.3390/polym11050760

Author Contributions

Vladimir E. Kuznetsov conceived and designed the experiments and wrote the paper; Azamat G. Tavitov and Oleg D. Urzhumtsev performed the experiments; Mikhail V. Mikhalin designed and made the testing apparatus; Alexey N. Solonin contributed analysis tools.

References

1. Wohlers, T. Wohlers Report 2016: 3D Printing and Additive Manufacturing State of the Industry Annual Worldwide Progress Report; Wohlers Associates Inc.: Fort Collins, CO, USA, 2016. [Google Scholar]
2. Frauenfelder, M. Make: Ultimate Guide to 3D Printing (2014). Maker Media.
3. https://formlabs.com/3d-printers/fuse-1/
4. Crump, S. Apparatus and method for creating three-dimensional objects. U.S. Patent 5121329, 30 October 1989.
5. Crump S., Fast, Precise, Safe Prototype with FDM, ASME PED, vol. 50 (1991), pp. 53-60
6. Crump S., The extrusion process of fused deposition modeling, – Proc. of 3rd Intl. Conf. on Rapid Prototyping, 1992
7. Sells, E.; Bailard, S.; Smith, Z.; Bowyer, A.; Olliver, V. RepRap: The Replicating Rapid Prototyper-Maximizing Customizability by Breeding the Means of Production. In Proceedings of the World Conference on Mass Customization and Personalization, Cambridge, MA, USA, 7–10 October 2007
8. https://reprap.org
9. Jones, R.; Haufe, P.; Sells, E.; Iravani, P.; Olliver, V.; Palmer, C.; Bowyer, A. RepRap-the Replicating Rapid Prototyper. Robotica **2011**, 29, 177–191
10. Bowyer, A. 3D Printing and Humanity's First Imperfect Replicator. 3D Print. Addit. Manuf. **2014**, 1, 4–5.
11. https://www.3dhubs.com/
12. R. Geyer, J. R. Jambeck, K. L. Law, Production, use, and fate of all plastics ever made. Sci. Adv. 3, e1700782 (2017). DOI: 10.1126/sciadv.1700782
13. Gershenfeld, N. How to make almost anything. Foreign Affairs 2012, 91, 6, 43-57
14. Gwamuri, J.; Wittbrodt, B.; Anzalone, N.; Pearce, J. Reversing the Trend of Large Scale and Centralization in Manufacturing: The Case of Distributed Manufacturing of Customizable 3-D-Printable Self-Adjustable Glasses. Chall. Sustain. **2014**, 2, 30–40.
15. Wittbrodt, B.; Laureto, J.; Tymrak, B.; Pearce, J. Distributed Manufacturing with 3-D Printing: A Case Study of Recreational Vehicle Solar Photovoltaic Mounting Systems. J. Frugal Innov. **2015**, 1, 1–7.
16. Woern, A.L.; Pearce, J.M. Distributed Manufacturing of Flexible Products: Technical Feasibility and Economic Viability. Technologies **2017**, 5, 71.
17. Petersen, E.E.; Kidd, R.W.; Pearce, J.M. Impact of DIY Home Manufacturing with 3D Printing on the Toy and Game Market. Technologies **2017**, 5, 45.
18. Petersen, E.E.; Pearce, J. Emergence of Home Manufacturing in the Developed World: Return on Investment for Open-Source 3-D Printers. Technologies **2017**, 5, 7.
19. Wittbrodt, B.T.; Glover, A.G.; Laureto, J.; Anzalone, G.C.; Oppliger, D.; Irwin, J.L.; Pearce, J.M. Life-cycle economic analysis of distributed manufacturing with open-source 3-D printers. Mechatronics **2013**, 23, 713–726.
20. Anderson, P.; Sherman, C.A. A discussion of new business models for 3D printing. Int. J. Technol. Mark. **2007**, 2, 280–294.
21. Laplume, A.; Anzalone, G.; Pearce, J. Open-source, self-replicating 3-D printer factory for small-business manufacturing. Int. J. Adv. Manuf. Technol. **2015**, 85, 633–642.
22. Laplume, A.; Petersen, B.; Pearce, J. Global value chains from a 3D printing perspective. J. Int. Bus. Stud. **2016**, 47, 595–609.

23. Rifkin, J. The Zero Marginal Cost Society: The Internet of Things, the Collaborative Commons, and the Eclipse of Capitalism; Palgrave Macmillan: Basingstoke, UK, 2014.
24. Pearce, J. Building Research Equipment with Free, Open-Source Hardware. Science **2012**, 337, 1303–1304.
25. Pearce, J. Open-Source Lab.: How to Build Your Own Hardware and Reduce Research Costs, 1st ed.; Elsevier: Waltham, MA, USA, 2014.
26. Baden, T.; Chagas, A.; Marzullo, T.; Prieto-Godino, L.; Euler, T. Open Laware: 3-D Printing Your Own Lab Equipment. PLoS Biol. **2015**, 13, e1002175.
27. Approaches to open source 3-D printable probe positioners and micromanipulators for probe stations https://doi.org/10.1016/j.ohx.2018.e00042
28. Oberloier, S.; Pearce, J.M. General Design Procedure for Free and Open-Source Hardware for Scientific Equipment. *Designs* **2018**, *2*, 2.
29. Petersen, E.E.; Kidd, R.W.; Pearce, J.M. Impact of DIY Home Manufacturing with 3D Printing on the Toy and Game Market. *Technologies* **2017**, *5*, 45.
30. https://www.nasa.gov/mission_pages/station/research/news/3Dratchet_wrench/
31. Wong, J.Y.; Pfahnl, A.C. 3D Printing of Surgical Instruments for Long-Duration Space missions. Aviat. Space Environ. Med. **2014**, 85, 758–763.
32. Pearce, J.M. Applications of open source 3-D printing on small farms. Org. Farming **2015**, 1, 19–35.
33. https://3dprint.com/tag/3d-printing-agricultural-uses/
34. Guido A.O. Adam, Detmar Zimmer, Design for Additive Manufacturing—Element transitions and aggregated structures, CIRP Journal of Manufacturing Science and Technology **2014**, 7, 1, 20-28. (https://doi.org/10.1016/j.cirpj.2013.10.001)
35. Hague R., Mansour S., Saleh N. Material and design considerations for rapid manufacturing, International Journal of Production Research **2004**, 42:22, 4691-4708, DOI: 10.1080/00207840410001733940
36. Pedro Miguel Cardoso Carneiro, Pedro Gamboa, (2019) "Structural analysis of wing ribs obtained by additive manufacturing", Rapid Prototyping Journal, https://doi.org/10.1108/RPJ-02-2018-0044
37. Rezaie, R., Badrossamay, M.Email Author, Ghaei, A., Moosavi, H. Topology optimization for fused deposition modeling process. Procedia CIRP, 6 (2013), pp. 521-526 https://doi.org/10.1016/j.procir.2013.03.098
38. Kuznetsov, V.E.; Solonin, A.N.; Urzhumtsev, O.D.; Schilling, R.; Tavitov, A.G. Strength of PLA Components Fabricated with Fused Deposition Technology Using a Desktop 3D Printer as a Function of Geometrical Parameters of the Process. *Polymers* **2018**, *10*, 313. https://doi.org/10.3390/polym10030313
39. Kuznetsov, V.E.; Solonin, A.N.; Tavitov, A.G.; Urzhumtsev, O.D.; Vakulik, A.H.. Increasing of Strength of FDM (FFF) 3D Printed Parts by Influencing on Temperature-Related Parameters of the Process. Preprints 2018, 2018030102 (doi: 10.20944/preprints201803.0102.v2).
40. Stephens B., Azimi P., Orch Z., Ramos T., Ultrafine particle emissions from desktop 3D printers,Atmospheric Environment,Volume 79, 2013,Pages 334-339 https://doi.org/10.1016/j.atmosenv.2013.06.050
41. West, C., McTaggart, R., Letcher, T., Raynie, D., & Roy, R. (2019). Effects of Gamma Irradiation upon the Mechanical and Chemical Properties of 3D-Printed Samples of Poly Lactic Acid. Journal of Manufacturing Science and Engineering, 1. doi:10.1115/1.4042581
42. Wittbrodt, B.; Pearce, J.M. The effects of PLA color on material properties of 3-D printed components. Add. Manuf. 2015, 8, 110–116